Supporting Information: Dynamic nuclear polarization in a magnetic resonance force microscope experiment

Corinne E. Isaac,[1] Christine M. Gleave,[1] Paméla T. Nasr,[1] Hoang L. Nguyen,[1] Elizabeth A. Curley,[1] Jonilyn L. Yoder,[1,*] Eric W. Moore,[1,†] Lei Chen,[1,‡] and John A. Marohn[1]

[1]*Department of Chemistry and Chemical Biology, Ithaca, New York 14853-1301, USA*

(Dated: February 1, 2016)

I. FREQUENCY NOISE AND EQUIVALENT FORCE NOISE

In the experiments described in the manuscript, electron-spin resonance and nuclear magnetic resonance were registered as a change in the mechanical resonance frequency of a cantilever. Thermo-mechanical position fluctuations place a fundamental limit on how small a cantilever frequency shift can be measured in a given averaging time.[1–4] In this section we present cantilever frequency-fluctuation power spectra and use these spectra to assess how close the experiments in the manuscript were to operating at the thermo-mechanical limit.

A power spectrum of cantilever frequency fluctuations $P_{\delta f_c}(f)$ was collected at $B_0 = 0.655$ T and $B_0 = 6$ T, in vacuum, at 4.2 K (see Fig. S1). Apparent in the spectrum are $\propto 1/f$ dielectric fluctuations at low offset frequency f[5] and detector noise $\propto f^2$ at high f.[3] The detector-noise contribution to the cantilever frequency-noise power spectrum is[3,4]

$$P^{\text{det}}_{\delta f_c}(f) = \frac{P^{\text{det}}_{\delta x}}{x^2_{\text{rms}}} f^2 \tag{1}$$

where x_{rms} is the root-mean-square cantilever amplitude and $P^{\text{det}}_{\delta x}$ is the power spectrum of detector noise expressed in units of equivalent position noise. The high-f data in Fig. S1 was fit to Eq. 1 to obtain $P^{\text{det}}_{\delta x} = 3.6 \times 10^{-6}\,\text{nm}^2\,\text{Hz}^{-1}$.

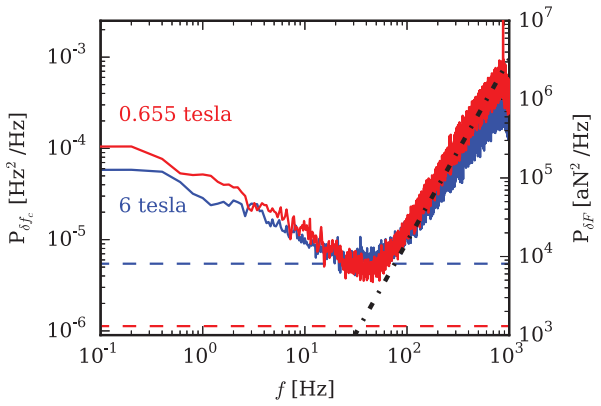

FIG. S1. Power spectrum of cantilever frequency fluctuations $P_{\delta f_c}$ versus offset frequency f at $B_0 = 0.655\,\text{T}$ (red line) and $B_0 = 6.0\,\text{T}$ (blue line). The $P_{\delta f_c}$ data above $f \geq 10^2$ Hz was fit to Eq. 1 with $x_{\text{rms}} = 69$ nm to obtain $P^{\text{det}}_{\delta x} = 3.6 \times 10^{-6}$ nm^2 Hz^{-1} (dotted black line), the power spectrum of detector noise expressed in units of equivalent position noise. The right-hand axis is $P_{\delta f_c}$ rewritten in terms of an equivalent force fluctuation using Eq. 10 and $k_c = 1.0$ mN m^{-1}, $f_c = 3500$ Hz, and x_{rms}. The dashed lines are the thermo-mechanical force fluctuations calculated from Eq. 11 at $B_0 = 0.655$ T (dashed red line), where the cantilever ringdown time $\tau_c = 0.94$ s, and at $B_0 = 6.0\,\text{T}$ (dashed blue line), where $\tau_c = 0.15\,\text{s}$. Other experimental parameters: temperature $T_0 = 4.2$ K, tip-sample separation $h = 1500$ nm, acquisition time $T_{\text{acq}} = 10\,\text{s}$ per average, and number of averages $n_{\text{avg}} = 32$.

The cantilever frequency fluctuations can be analyzed, as follows, to obtain a power spectrum of equivalent force fluctuations. Fluctuating forces acting on the cantilever lead to fluctuations in the cantilever position whose power spectrum is given by

$$P_{\delta x}(f) = \frac{P_{\delta F}(f)}{k_c^2} \frac{f_c^4}{(f_c^2 - f^2)^2 - f^2 f_c^2/Q^2} \tag{2}$$

where $P_{\delta F}(f)$ is the power spectrum of force fluctuations and k_c, f_c, and Q are the cantilever spring constant, resonance frequency, and quality factor, respectively. These fluctuations in cantilever position contribute noise to the measured cantilever frequency. The resulting power spectrum of induced frequency fluctuations is given by

$$P_{\delta f_c}(f) = \frac{f^2}{2\,x^2_{\text{rms}}} \left(P_{\delta x}(f + f_c) + P_{\delta x}(f - f_c)\right). \tag{3}$$

We could at this point substitute Eq. 2 into Eq. 3 and obtain a relation between $P_{\delta f_c}$ to $P_{\delta F}$. Before doing so, it is helpful to examine

$$P_{\delta x}(f \pm f_c) = \frac{P_{\delta F}(f \pm f_c)}{k_c^2} \times \frac{f_c^4}{(f_c^2 - (f \pm f_c)^2)^2 - (f \pm f_c)^2 f_c^2/Q^2}, \tag{4}$$

which simplifies to

$$P_{\delta x}(f \pm f_c) \approx \frac{P_{\delta F}(f \pm f_c)}{k_c^2} \frac{f_c^4}{4f^2 f_c^2 + f_c^4/Q^2} \tag{5}$$

where in going from Eq. 4 to Eq. 5 we have used that $f \ll f_c$.

Substituting Eq. 5 into Eq. 3 yields

$$P_{\delta f_c}(f) = \frac{f_c^2}{k_c^2\, x_{\rm rms}^2} \times \frac{1}{2}\left(P_{\delta F}(f_c + f) + P_{\delta F}(f_c - f)\right) \times \frac{f^2 f_c^2}{4f^2 f_c^2 + f_c^4/Q^2} \quad (6)$$

where we have used that $P_{\delta F}(f)$ is an even function of f to write $P_{\delta F}(f \pm f_c) \rightarrow P_{\delta F}(f_c \pm f)$. This expression may be simplified further by defining

$$P_{\delta F}^{\rm avg}(f_c, f) = \frac{1}{2}\left(P_{\delta F}(f_c + f) + P_{\delta F}(f_c - f)\right), \quad (7)$$

the average power spectrum of force fluctuations at an offset frequency f below and f above the cantilever frequency. Substituting Eq. 7 into Eq. 6 gives

$$P_{\delta f_c}(f) = \frac{f_c^2}{4\, k_c^2\, x_{\rm rms}^2} P_{\delta F}^{\rm avg}(f_c, f) \frac{1}{1 + f_c^2/(4f^2Q^2)}. \quad (8)$$

The last term in Eq. 8 becomes 1 in the limit that $f \gg f_c/(2Q)$, that is, when f is larger than the width of the oscillator resonance in cycles s^{-1}. In this limit,

$$P_{\delta f_c}(f) = \frac{f_c^2}{4\, k_c^2\, x_{\rm rms}^2} P_{\delta F}^{\rm avg}(f_c, f). \quad (9)$$

Solving for $P_{\delta F}^{\rm avg}$ we obtain

$$P_{\delta F}^{\rm avg}(f_c, f) = \frac{4\, k_c^2\, x_{\rm rms}^2}{f_c^2} P_{\delta f_c}(f). \quad (10)$$

If the *only* source of frequency noise was the underlying force noise, then we could use Eq. 10 to calculate the fluctuating forces driving the cantilever from the measured power spectrum of cantilever frequency fluctuations. In practice, however, $P_{\delta f_c}(f)$ contains additional contributions from surface noise and detector noise. Applying Eq. 10 to the measured frequency fluctuations we obtain an *equivalent* or *effective* power spectrum of force noise. In this case Eq. 10 can be interpreted as the power spectrum of force fluctuations that, when applied to the cantilever, would yield frequency fluctuations having the observed power spectrum $P_{\delta f_c}$. The $P_{\delta F}^{\rm avg}$ calculated in this way is shown as the right-hand y axis in Fig. S1.

For comparison, we can plot the power spectrum of thermo-mechanical force fluctuations $P_{\delta F}^{\rm therm}$. This power spectrum is independent of frequency. In terms of measured parameters,

$$P_{\delta F}^{\rm therm} = \frac{2 k_{\rm B} T_0 k_c}{\pi^2 f_c^2 \tau_c} \quad (11)$$

where $k_{\rm B}$ is Boltzmann's constant, T_0 is temperature, and τ_c is the cantilever ringdown time. Comparing the observed $P_{\delta F}^{\rm avg}$ data in Fig. S1 to the calculated $P_{\delta F}^{\rm therm}$, we see that the equivalent force noise at $B_0 = 6.0$ T was near the thermo-mechanical limit at offset frequencies 20 Hz $< f <$ 50 Hz while at $B_0 = 0.655$ T the equivalent force noise was never better than $10\times$ the thermo-mechanical limit.

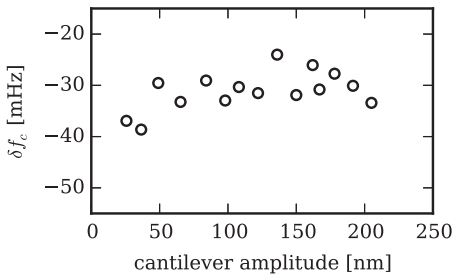

FIG. S2. DNP-enhanced ^{1}H spin signal versus peak-to-peak cantilever ampltitude. Experimental parameters: $B_0 = 0.655$ T, $h = 1500$ nm, $f_{\rm MW} = 18.5$ GHz, irradiation time $\tau = 20$ s, $f_{\rm rf} = 27.5$ MHz, $\Delta f_{\rm rf} = 1$ MHz.

II. EFFECT OF CANTILEVER MOTION ON THE DNP SIGNAL

During the NMR, ESR, and DNP experiments described in the manuscript, the cantilever was oscillated at its resonance frequency. According to Eq. 9, cantilever root-mean-square frequency noise is inversely proportional to cantilever amplitude. Moreover, in the ESR experiment some cantilever motion is required to scan the resonant slice through the sample and bring a measurably large number of electron spins into resonance.

The microwave induced ^{1}H spin signal was found to be independent of the peak-to-peak displacement of the cantilever as seen in Fig. S2. This observation is consistent with the manuscript's finding that the nuclear spins are polarized in a thin region on the proximal and distal sides of the resonant slice. Oscillating the cantilever in the x direction causes a lateral blurring of the resonant slice but does not, to first order, change location or thickness of the slice in the z direction. Consequently, increasing the oscillation amplitude of the cantilever should not cause any cancellation of the DNP enhancement.

III. COPLANAR WAVEGUIDE DETAILS

The coplanar waveguide consisted of two sections — a copper CPW on an Arlon substrate and a copper CPW fabricated on high resistivity silicon.

Arlon section — The CPW-on-Arlon section was purchased from PCB Fab Express with precut holes to facilitate making a connection to an SMA coaxial connector. The Arlon substrate had a thickness of $H = 2540$ μm and a (specified) relative permittivity of $\epsilon_r = 9.8$. The waveguide was made of 35 μm thick copper. The waveguide's center line was

frequency	parameter	measured	simulated
210 MHz	S_{21}	−1.1 dB	−0.95 dB
210 MHz	S_{11}	−19.0 dB	−19.6 dB
17 GHz	S_{21}	−17 dB	−1.2 dB
17 GHz	S_{11}	−12 dB	−13.2 dB

TABLE S1. Coplanar waveguide scattering parameters measured at room temperature in air and simulated using SONNET.

$w = 457$ μm wide and the gap to the flanking ground plane was $s = 228.6$ μm wide on each side. A 10 mm by 2 mm section was removed from the center of the Arlon substrate to accommodate the CPW-on-Si section described below.

Silicon section — The CPW-on-Si section of the waveguide was microfabricated at the Cornell Nanoscale Science and Technology Facility. The substrate was made of high-resistivity silicon, had a thickness of $H = 500$ μm, and had a (specified) relative permittivity of $\epsilon_r = 11.8$. The waveguide was made of 0.2 μm thick copper. The waveguide's outer center line was $w = 480$ μm wide and the gap to the flanking ground plane was $s = 230$ μm on each side. This section tapered, over a distance of 450 μm, to a narrower waveguide; the w/s ratio was maintained in the tapered region. The narrower, "microwire" section of coplanar waveguide was $L = 500$ μm long, $w = 10$ μm wide, and had an $s = 6$ μm gap. The dimensions of the 10 mm by 2 mm hole in the CPW-on-Arlon section were precisely measured, and the CPW-on-Si was cut using a dicing saw to fit into the hole leaving less than a 200 μm gap between the two sections.

Connections — The two CPWs were connected *via* wire bonds. Three wire bonds were used to connect the center line and three wire bonds were used to connect each of the flanking ground planes.

***S* parameters** — See Table S1 for measured and calculated scattering parameters.

IV. ADIABATICITY OF NUCLEAR SPIN INVERSIONS

The CPW described above was designed to deliver broadband irradiation. Electromagnetic simulations (Sonnet Software, Inc.) predicted a transverse magnetic field strength B_1 of 2.5 mT with only 200 mW of input power at frequencies below 5 GHz where simulated and measured scattering parameters agreed within 1 dB. To invert the nuclear magnetization reversibly, the nuclear spin magnetization must stay aligned with the effective field in the rotating frame during an adiabatic rapid passage through resonance. Maintaining this alignment requires a B_1 large enough to meet the adiabatic condition,

$$B_1^2 \gg \frac{1}{2\pi\gamma}\frac{d}{dt}\Delta B_0 \tag{12}$$

with $d\Delta B_0/dt$ the rate of change in the magnetic field and $\gamma = 42.56$ MHz T^{-1} the ^{1}H gyromagnetic ratio. According to Eq. 12, a transverse magnetic field of strength $B_1 = 2.5$mT should meet the adiabatic condition during a $\Delta f_{rf} = 1$ MHz sweep as long as the sweep duration Δt_{rf} was ≥ 0.014 ms.

Harrell *et al.* provide guidelines that allow us to further quantify how efficiently we are inverting nuclear spins.[6] Considering a spin-1/2 system and a finite radiofrequency sweep rate, one can calculate the probability that spins undergo a diabatic transition rather than an adiabatic transition using

$$P = \exp\left(\frac{-(2\pi\gamma\ B_1)^2}{4\,|d\ f_{rf}/dt|}\right). \tag{13}$$

Under our experimental conditions, we calculate a 10% likelihood of a diabatic transition with a $\Delta f_{rf} = 1$ MHz sweep lasting $\Delta t_{rf} = 0.021$ ms.

Equation 13 is valid in the limit that $\Delta f_{rf} \geq 5\gamma B_1$. This condition sets a lower limit on the width of an ARP frequency sweep necessary to prevent projection losses — losses incurred from projecting the magnetization on the effective field when the rf is turned on. For $B_1 = 2.5$ mT, the 1 MHz wide frequency sweep used throughout these experiments should be adequate. The $\Delta f_{rf} = 0.3$ MHz ARP sweeps used to map the DNP enhancement, however, do not strictly satisfy this condition. The signal from the 0.3 MHz sweeps was likely affected by (modest) projection losses.

The applied sweeps in our experiments were 0.28 to 2.8 ms in duration – sufficient, we predicted, to meet the adiabatic condition with negligible diabatic transitions and projection losses. After applying consecutive adiabatic rapid passage sweeps through resonance, however, we did not observe a complete return of the cantilever resonance frequency to its initial value (see the experiments and data presented in Fig. S3). Figure S3(a) shows the percent return of the cantilever frequency to its initial value following two identical ARP sweeps with a two second delay between them. The fidelity of the inversions is poor. Three hypotheses were developed to explain the observation:

1. the oscillating field was not as strong as predicted; thus, we were not meeting the adiabatic condition;
2. a short $T_{1\rho}$ was causing a loss of magnetization during the rf sweep; and
3. spin diffusion was moving polarized spins out of the resonant slice during the delay before the second rf sweep was applied to re-invert the spins.

As the duration of the sweep was shortened, the percent return improved, indicating that we were likely meeting the adiabatic condition but were possibly losing magnetization due to

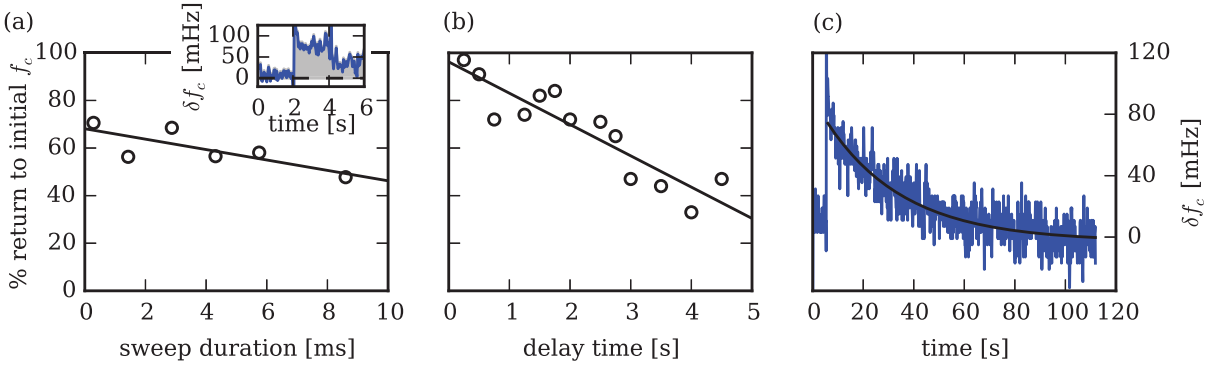

FIG. S3. The percent return of the cantilever resonance frequency following the application of two ARP sweeps applied to invert the sample's ^{1}H magnetization. (a) Percent return versus the duration of the sweep, $\Delta t_{\rm rf}$, with the delay between the sweeps fixed at 2 s. (b) Percent return versus the delay between the sweeps, with the sweep duration fixed at $\Delta t_{\rm rf} = 0.28$ ms. (c) The cantilever frequency shift following a single $\Delta t_{\rm rf} = 0.28$ ms duration sweep. The solid black line is a fit to an exponential decay with time constant $T_1 = 30.9 \pm 0.9$ s. Experimental parameters: $B_0 = 4.93$T, $h = 1500$ nm, $f_{\rm rf} = 210$ MHz, $\Delta f_{\rm rf} = 1$ MHz, and $B_1 = 2.5$ mT (estimated).

a short $T_{1\rho}$. Fig. S3(b) shows that the percent return improves as the inter-sweep delay is decreased. Fig. S3(c) shows a real-time measurement of the ^{1}H spin-lattice relaxation time; the measured $T = 30.9 \pm 0.9$ s is considerably longer than the few-second lifetime of the inverted magnetization apparent in Fig. S3(b). Taken together, these findings support the hypothesis that spin diffusion is carrying the inverted spin polarization away from the resonant slice on the time scale of just a few seconds.

V. ABSOLUTE NUCLEAR SPIN POLARIZATION

The experiment described in this manuscript is the first time that microwave-assisted DNP has been definitively demonstrated in an MRFM experiment. A 10 to 20-fold ^{1}H polarization enhancement was achieved. Figure S4 summarizes the absolute polarization and buildup time achieved in inductively-detected DNP experiments carried out at temperatures ranging from $T_0 = 4.2$ K to $T_0 = 7$ K. The significantly greater enhancements achieved in these previous DNP experiments often came at the expense of long polarization buildup times. The buildup time of $\tau \sim 13$ s seen in this experiment is favorably low compared to prior inductively-detected low temperature DNP experiments. Implementing more optimized polarizing agents,[7–11] freezing the sample in a partially deuterated glass-forming solvent matrix, and operating at higher fields should lead to significantly greater absolute ^{1}H polarization in the MRFM experiment.

VI. AUTHOR CONTRIBUTIONS

Short summary — Author contributions: C.E.I. and J.A.M. designed the research; E.W.M., J.L.Y., and L.C. designed and built the microscope; L.C., J.L.Y., C.M.G., C.E.I. and H.L.N. cold-tested and characterized the microscope; C.M.G. and P.T.N. fabricated coplanar waveguides; P.T.N fabricated cantilevers; C.E.I., H.L.N., and E.A.C. developed experimental protocols; C.E.I. performed the research; and C.E.I. and J.A.M. analyzed data and co-wrote the manuscript.

Long summary —

- Corinne E. Isaac: cold-tested the microscope; characterized and optimized the Pan walkers; developed alignment protocols; designed and simulated the current version of the coplanar waveguide; performed experiments; analyzed data; and co-wrote manuscript
- Christine M. Gleave: cold-tested the microscope; designed, simulated and fabricated initial versions of coplanar waveguides
- Paméla T. Nasr: fabricated the cantilever and CPW; fabricated grids for aligning the cantilever to the CPW
- Hoang Long Nguyen: aided in cold-testing the microscope; helped develop alignment protocol
- Elizabeth A. Curley: helped develop alignment protocol
- Eric W. Moore: co-designed and co-built the microscope superstructure
- Jonilyn L. Yoder: co-designed and co-built the microscope superstructure, cold-tested the microscope
- Lei Chen: built the Pan-style walkers; designed the probe head; assembled and performed initial cold-testing of the probe head and microscope
- John A. Marohn: designed experiments; analyzed data; and co-wrote manuscript

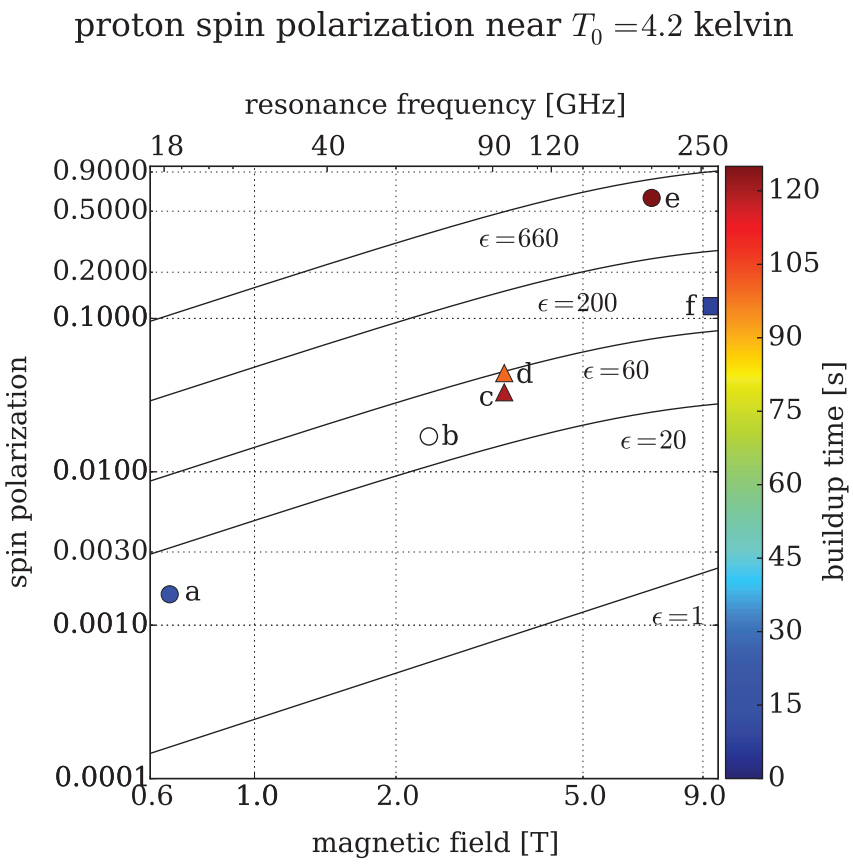

FIG. S4. Proton spin polarization achievable *via* dynamic nuclear polarization at $T_0 = 4.2$ K as a function of magnetic field, for representative enhancement factors ranging from $\epsilon = 1$ (no enhancement; lower curve) to $\epsilon = 660$ (full enhancement; upper curve). At full enhancement, the proton polarization is equal to the electron spin polarization. Also plotted is the absolute ^{1}H polarization achieved in previous low-temperature DNP experiments: (a) this experiment, (b) Ref. 7, (c) Ref. 8, (d) Ref. 9, (e) Ref. 10, and (f) Ref. 11. The marker type indicates the operating temperature: circles for $T_0 = 4.2$ K, triangles for $T_0 = 6$ K, and squares for $T_0 = 7$ K. The fill color indicates the nuclear magnetization buildup time; see the legend on the right-hand side of the plot. The buildup time for experiment (b) is unknown.

VII. NOTES AND REFERENCES

* née Longenecker. Present address: Quantum Information and Integrated Nanosystems Group, Lincoln Laboratory, Massachusetts Institute of Technology, Lexington, Massachusetts 02420-9108, USA
† Present address: Department of Chemistry, Lehigh University, Bethlehem, Pennsylvania 18015, USA
‡ Present address: State Key Laboratory of Functional Materials for Informatics, Shanghai Institute of Microsystem and Information Technology, Chinese Academy of Sciences, Shanghai, China

[1] T. R. Albrecht, P. Grutter, D. Home and D. Rugar, Frequency modulation detection using highQ cantilevers for enhanced force microscope sensitivity, *J. Appl. Phys.*, 1991, **69**, 668 [doi:10.1063/1.347347].
[2] Y. Obukhov, K. C. Fong, D. Daughton and P. C. Hammel, Real time cantilever signal frequency determination using digital signal processing, *J. Appl. Phys.*, 2007, **101**, – [doi:10.1063/1.2434955].
[3] S. M. Yazdanian, J. A. Marohn and R. F. Loring, Dielectric Fluctuations in force microscopy: Noncontact friction and frequency jitter, *J. Chem. Phys.*, 2008, **128**, 224706 [doi:10.1063/1.2932254].
[4] R. P. Dwyer and J. A. Marohn, *The FreqDemod 0.2.1 Python package*, Available for installation at https://pypi.python.org/pypi/FreqDemod. Documentation available at http://freqdemod.readthedocs.org. Source code available at https://github.com/JohnMarohn/FreqDemod., 2015.
[5] S. M. Yazdanian, N. Hoepker, S. Kuehn, R. F. Loring and J. A. Marohn, Quantifying Electric Field Gradient Fluctuations over Polymers Using Ultrasensitive Cantilevers, *Nano Lett.*, 2009, **9**, 2273 – 2279 [doi:10.1021/nl9004332].
[6] L. E. Harrell, Cantilever noise in off-cantilever-resonance force-detected nuclear magnetic resonance, *J. Appl. Phys.*, 2004, **95**, 2577 – 2581 [doi:10.1063/1.1643780].
[7] H. Cho, J. Baugh, C. A. Ryan, D. G. Cory and

C. Ramanathan, Low temperature probe for dynamic nuclear polarization and multiple-pulse solid-state NMR, *J. Magn. Reson.*, 2007, **187**, 242 – 250 [doi:http://dx.doi.org/10.1016/j.jmr.2007.04.012].

[8] D. Shimon, A. Feintuch, D. Goldfarb and S. Vega, Static ^{1}H dynamic nuclear polarization with the biradical TOTAPOL: A transition between the solid effect and the cross effect, *Phys. Chem. Chem. Phys.*, 2014, **16**, 6687–6699 [doi:10.1039/C3CP55504F].

[9] D. Shimon, Y. Hovav, A. Feintuch, D. Goldfarb and S. Vega, Dynamic nuclear polarization in the solid state: A transition between the cross effect and the solid effect, *Phys. Chem. Chem. Phys.*, 2012, **14**, 5729 [doi:10.1039/c2cp23915a].

[10] T. A. Siaw, S. A. Walker, B. D. Armstrong and S.-I. Han, Inductively Coupled NMR Probe for Versatile Dynamic Nuclear Polarization Operation at 7 T: Observation of $61\pm2\%$ ^{1}H Polarization at 4 K, *J. Magn. Res.*, 2012, **221**, 5 – 10 [doi:10.1016/j.jmr.2012.05.017].

[11] K. R. Thurber, W.-M. Yau and R. Tycko, Low-temperature dynamic nuclear polarization at 9.4 T with a 30 mW microwave source, *J. Magn. Res.*, 2010, **204**, 303 – 313 [doi:10.1016/j.jmr.2010.03.016].